



HAL
open science

Nature of the Ba $4d$ Splitting in BaTiO₃ unraveled by a combined experimental and theoretical study

Pierre-Marie Deleuze, H el ene Magnan, Antoine Barbier, Zheshen Li, Alberto Verdini, Luca Floreano, Bruno Domenichini, C eline Dupont

► **To cite this version:**

Pierre-Marie Deleuze, H el ene Magnan, Antoine Barbier, Zheshen Li, Alberto Verdini, et al.. Nature of the Ba $4d$ Splitting in BaTiO₃ unraveled by a combined experimental and theoretical study. *Journal of Physical Chemistry C*, 2022, 126 (37), pp.15899-15906. 10.1021/acs.jpcc.2c02510 . hal-03795651

HAL Id: hal-03795651

<https://hal.science/hal-03795651>

Submitted on 17 Nov 2022

HAL is a multi-disciplinary open access archive for the deposit and dissemination of scientific research documents, whether they are published or not. The documents may come from teaching and research institutions in France or abroad, or from public or private research centers.

L'archive ouverte pluridisciplinaire **HAL**, est destin ee au d ep ot et  a la diffusion de documents scientifiques de niveau recherche, publi es ou non,  emanant des  tablissements d'enseignement et de recherche fran ais ou  trangers, des laboratoires publics ou priv es.

The nature of the Ba $4d$ splitting in BaTiO₃ unraveled by a combined experimental and theoretical study

Pierre-Marie Deleuze,[†] H el ene Magnan,^{‡,||} Antoine Barbier,^{‡,||} Zheshen Li,[¶]
Alberto Verdini,[§] Luca Floreano,[§] Bruno Domenichini,^{†,||} and C eline Dupont^{*,†,||}

[†]*Laboratoire Interdisciplinaire Carnot de Bourgogne (ICB), UMR 6303 CNRS, Universit e
Bourgogne Franche-Comt e, BP 47870, 21078 Dijon Cedex, France*

[‡]*Universit e Paris Saclay, CEA, CNRS, Service Physique Etat Condense (SPEC), F-91191
Gif Sur Yvette, France*

[¶]*ISA, University of Aarhus, Ny Munkegade, DK-8000, Aarhus C, Denmark*

[§]*Instituto Officina dei Materiali IOM-CNR, Laboratorio TASC s.s. 14 km 163.5, 34149
Trieste, Italy*

^{||}*FR SPE 2050 CNRS*

E-mail: celine.dupont@u-bourgogne.fr

Abstract

In this paper, synchrotron radiation photoemission techniques are used to unravel the pending nature of the two Ba $4d$ components, also observed on Ba $3d$ lines, and commonly named Ba(α) and Ba(β). Investigations were carried out on the (001) surface of epitaxial very thin (≤ 20 nm) films combined with DFT calculations. Photoelectron diffraction experiments reveal different behaviors for Ba(α) and Ba(β) components. While six well defined diffraction features corresponding to the BaTiO₃ bulk structure are observed for the Ba(α) component, no feature really appears in the diffraction pattern of Ba(β). This observations reveal the absence of forward scattering processes, hence this component comes mostly from surface BaO plane. Supporting these results, DFT calculations demonstrate a shift to lower binding energy (BE) only for the Ba $4d$ peak from the topmost BaO layer with respect to the photoelectron peak stemming from bulk layers. Hence, only one peak (the Ba(α) one) should be observed for a sample with a complete TiO₂ termination. This hypothesis is supported by photoemission measurements carried out at low photon energy in grazing angle emission, in order to enhance the signal from topmost layers with respect to the bulk. For each sample, the Ba(β)/Ba(α) intensity ratio is well reproduced by a model where the Ba(β) signal is only coming from the topmost surface BaO plane.

Introduction

Surfaces define the interface between a material and an external medium that may be as various as vacuum, air or electrolyte. For many technological important processes, the interaction of the surface with the medium is of major importance and in some cases the nature of the most external layer even dominates the whole process. It has been evidenced in a number of studies that the extreme surface may dramatically affect the macroscopic properties of a material. For example, the adsorption behavior of a Cu(111) surface can be controlled by a low O-precovering,¹ while for Pt(110) the rate of CO oxidation can be modified by the presence of a surface oxide.² This general trend is also especially important for oxide surfaces. Hence, exchanging surface cation Bi by Co in BiVO₄ photoanodes leads to enhanced photocurrent density with superior stability;³ polar orientations of crystals can be stabilized by top surface reconstructions or metallic configurations;^{4,5} oxide surfaces may exhibit terminations dependent on the oxygen potential⁶ and even the magnetic ordering of a material may be influenced primarily by the surface magnetic long range ordering provided that its ordering temperature is lower than in the bulk.⁷ Generally speaking, the precise knowledge of the extreme surface configuration appears as a major issue and deserves detailed investigation since it can dramatically affect the macroscopic properties of a material. Here we aim at resolving the puzzling and long-standing case of the terminal surface configuration of BaTiO₃, a highly interesting material owing to its ferroelectric nature. Indeed, barium titanate was the first ceramic material discovered exhibiting ferroelectricity.⁸ Over the years, it has gained a lot of attention for its potential use in many technological applications, such as non-volatile memory devices, capacitors or photocatalysts. Given the importance of this material, it is noteworthy to get a deep understanding of its structural properties, since the fine characteristics of its surface (structure and chemical composition) will directly influence ferroelectric polarisation screening phenomena, surface catalysis, ... In this framework, X-ray photoelectron spectroscopy (XPS) is a powerful technique of surface characterization. In particular, when XPS is applied to BaTiO₃ samples, as Ba is a heavy element ($Z=56$), the

$3d$ and $4d$ bands appear as doublets because of spin-orbit coupling. However, in BaTiO_3 , each signal is further split into two components whose origin is not yet fully understood. Indeed, despite numerous studies devoted to this system no consensus has been reached on the origin of this core level split, which hampers the determination of the oxidation state and coordinative environment of involved barium atoms. The first study on this subject is the one of Hudson *et al.*⁹ who assigned the two components to surface and bulk Ba atoms. This assignment has been adopted several times,¹⁰⁻¹² but no study has yet provided a clear assignment between the binding energy (BE) of the peaks (high and low) and the position (exact depth) of the Ba atom. Besides, other studies have attributed the high BE component to surface contamination, more particularly to BaCO_3 species.¹³⁻¹⁵ Finally, some recent papers have rather associated this peak with Ba atoms in a higher oxidation state, namely corresponding to BaO_2 species.¹⁶⁻¹⁹ To improve the understanding of BaTiO_3 surface and thus to be able to precisely study important characteristics of this system such as interaction with adsorbates or reactivity, it is essential to disclose unambiguously the nature of the Ba $3d$ and $4d$ core level split in BaTiO_3 compounds.

For this purpose, a single crystal sample is ideally suited to perform spectroscopic and structural measurements aimed at an accurate modeling of the material. However, a BaTiO_3 single crystal would be highly insulating, limiting the spectroscopic studies using high fluence radiation such as synchrotron radiation. Nevertheless, it is possible to prepare epitaxial thin films of BaTiO_3 by atomic oxygen assisted molecular beam epitaxy (OA-MBE) on $\text{SrTiO}_3(001)$ ¹⁶ or $\text{Pt}(001)$ ²⁰ substrates. Such films are model materials, *i.e.* their orientation and crystallinity are well controlled, while their small thickness (typically less than 20 nm) allows to limit and evacuate the detrimental charge build-up potentially caused by photoemission process.

The aim of this work is to establish the origin of the still puzzling existence of two distinct components in the photoemission signals of Ba (in the present case, the $4d$ core level) from accurate spectroscopic studies associated with DFT calculations. We focused on the (001)

surface orientation, which corresponds to a stacking of BaO and TiO₂ planes. In order to enhance the structural effects on spectroscopic measurements, we synthesized samples with different types of terminations, which are further analyzed either by photoelectron diffraction (PED) or by synchrotron radiation photoemission spectroscopy (SR-PES) carried out at low photon energy and in grazing emission in order to enhance the surface sensitivity. The experimental evidences are coupled with DFT calculations to identify unequivocally the origin of the splitting.

Methods

Experimental

The 1% Nb doped SrTiO₃(001) substrates 5×5 mm squares with a thickness of 1 mm were provided, cut and polished by Crystal GmbH (Berlin, Germany) and the Pt(001) (10 nm diameter and thickness of 1mm) by Matek (Germany). Barium titanate is deposited by OA-MBE which allows the deposition of single crystalline layers of controlled morphology, stoichiometry and thickness. Dedicated Knudsen cells are used to evaporate high-purity Ba and Ti (99.99% grade) metals in the presence of an atomic oxygen plasma (high brilliance, 350 W power). Well-defined oxides are obtained under good vacuum conditions (10⁻⁷ mbar working pressure, 10⁻¹⁰ mbar base pressure). In order to clean the substrate prior to deposition, Nb:SrTiO₃ or Pt is first heated 1h at 450°C under oxygen plasma, with a filament located behind the sample. The sample is heated at 450°C during the growth. Five different samples were prepared with different thicknesses and surface terminations. For this purpose, the Ba and Ti molecular beams are stopped simultaneously (for one sample) to try to synthesize a stoichiometric surface or staggered (for 2 samples the Ti beam is stopped before the Ba one and conversely for the two other samples) to obtain surfaces enriched in one or the other cation. The range order of all these surfaces is controlled by RHEED at the end of the preparation. The characteristics and denominations of the samples are summarized

in Table 1.

Table 1: Thickness and theoretical termination of the studied samples. All samples are deposited on Nb:SrTiO₃(001) substrate, except S(0) deposited on Pt(001).

Name	Substrate	Thickness (nm)	Surface
S(Ti_1)	Nb:SrTiO ₃ (001)	10	Ti-rich
S(Ti_2)	Nb:SrTiO ₃ (001)	16	Ti-rich
S(0)	Pt(001)	20	stoichiometric
S(Ba_1)	Nb:SrTiO ₃ (001)	10	Ba-rich
S(Ba_2)	Nb:SrTiO ₃ (001)	16	Ba-rich

PED experiments have been performed at the ALOISA beamline²¹ of the ELETTRA Synchrotron Light Source in Trieste, Italy, in an ultra-high vacuum chamber (base pressure 10⁻¹⁰ mbar) previously described. The sample is prepared through an annealing (400 °C) under O₂ (10⁻⁶ mbar) for 50 min. After such a treatment, adventitious carbon peak is no more detectable. For photoemission and PED experiments, the X-ray beam is impinging the sample at grazing incidence (4°) in transverse magnetic polarization (quasi p-polarization). Surface analysis is performed by photoemission from Ba 4*d* and Ti 3*p* levels at a primary photon energy of 547 eV and 493 eV, respectively. This allows to measure the photoelectrons at the same kinetic energy of 455 eV, hence with the same escape depth. This electron energy is sufficiently low to provide an overall surface sensitivity, but large enough to allow the processes of forward scattering to dominate the photoelectron diffraction pattern, as compared to the processes of photoelectron back scattering. With this choice, we may differentiate more easily the processes coming from the topmost atomic layer from those coming from the buried ones (see experimental results section). PED patterns were recorded by scanning the azimuthal angle ϕ over *ca.* 120° including both symmetry directions [110] and [100]. The polar angle θ varies from -2 to 80°, where the surface normal corresponds to $\theta=0^\circ$. The step increment is set to 2° for both θ and ϕ . In order to obtain the full ϕ range of 360°, the measured patterns are folded symmetrically according to the C_{2v} point symmetry of the surface. The azimuthal orientation of the surface symmetry directions was first checked for a few Ba 4*d* PED scans at constant polar (emission) angles on a wider ϕ

range. The PED patterns are reported as χ functions with:

$$\chi(\theta, \phi) = \frac{I(\theta, \phi) - I_0(\theta)}{I_0(\theta)} \quad (1)$$

where $I_0(\theta)$ is given by the ϕ -average of the photoemission intensity $I(\theta, \phi)$ measured at polar angle θ and azimuth ϕ and takes effectively into account for the non-diffractive isotropic contribution.²²

SR-PES experiments have been carried out at the Aarhus storage ring in Denmark (ASTRID2) on the MATLINE beamline, dedicated to surface analysis and equipped with a SX700 grating monochromator. The end-station consists of μ -metal UHV chamber, a hemispherical SCIENTA SES-200 electron energy analyzer and a channelplate as detector. Sample preparation is similar to that performed for the sample analyzed in PED. All data were obtained with a pass energy of 20 eV and with a 100- μ m slit at grazing emission (15° from the sample surface) with p-polarized photons incident onto the sample at an angle of 50°. The photon energies were 110 eV for collecting of Ti 3*p* lines and 160 eV for Ba 4*d* lines. These energies lead to the same kinetics energy for Ti 3*p* and Ba 4*d* electrons (70-75 eV range), and thus to the same inelastic mean free path (IMFP). This allows to analyze the same material thickness for Ti and Ba. Besides, this avoids any problem of non-linearity of the analyzer. Overall resolution is around 60 meV at 75 eV (Ba 4*d* spectra). The base pressure during data acquisition was 10⁻¹⁰ mbar. All measurements were done at room temperature. Shirley background removal and Gaussian-Lorentzian (70-30) line shapes are used for all the peak area measurements.

Computational details

Density Functional Theory (DFT) calculations have been performed using the Vienna ab initio simulation package (VASP)^{23,24} under periodic boundary conditions. The electron-ion interaction is described within the projector-augmented plane-wave (PAW) method^{25,26} with

a kinetic energy cutoff of 500 eV and the inclusion of ten valence electrons for Ba, six for O and 4 for Ti. The generalized gradient approximation (GGA) is employed with the Perdew-Burke-Ernzerhof (PBE)²⁷ exchange correlation functional. The DFT+U approach is used by including an on-site Coulomb repulsion U-term for the Ti-3d electron, according to the Dudarev method.²⁸ The effective parameter $U_{\text{eff}} = 3.5$ eV is applied, allowing the band gap to increase to 2.23 eV, getting closer to the experimental value of 3.2 eV.²⁹ The convergence threshold on total energy is set to 10^{-6} eV. The structural optimization is stopped when the forces converged below $0.01 \text{ eV} \cdot \text{\AA}^{-1}$, while a $7 \times 7 \times 1$ Monkhorst-Pack³⁰ k-point mesh is used to sample the first Brillouin zone.

BaTiO₃(001), named BTO in the following, is modeled by a (1×1) unit cell reported on Figure 1, with $a=b=4.006 \text{ \AA}$, according to bulk parameters previously obtained.³¹ Eleven layers symmetric slabs are considered for both TiO₂ and BaO terminations, with a vacuum space of 20 \AA along the z axis. All atoms are allowed to relax. Core level binding energy (CLBE) shifts are calculated in the final state approximation according to the model developed by Köhler *et al.*³² In this method, the screening by the core electrons is not considered (frozen ground state PAW potentials for the excited state), hence we cannot obtain absolute values for CLBE. However, as demonstrated by Köhler *et al.*,³² accurate CLBE differences can be calculated.

Results and discussion

PED results

Figure 2(a) shows the Ba 4d spectrum obtained from sample S(0) with an excitation photon energy of 547 eV. This photon energy allows to obtain a kinetic energy of the detected electrons centered around 455 eV, *i.e.* an energy for which IMFP of the electrons is 1.15 nm for BaTiO₃ according to the TPP-2M formula.³³ This value of the IMFP allows an analysis including the topmost surface and a few atomic layers beneath. The Ba 4d lines can be de-

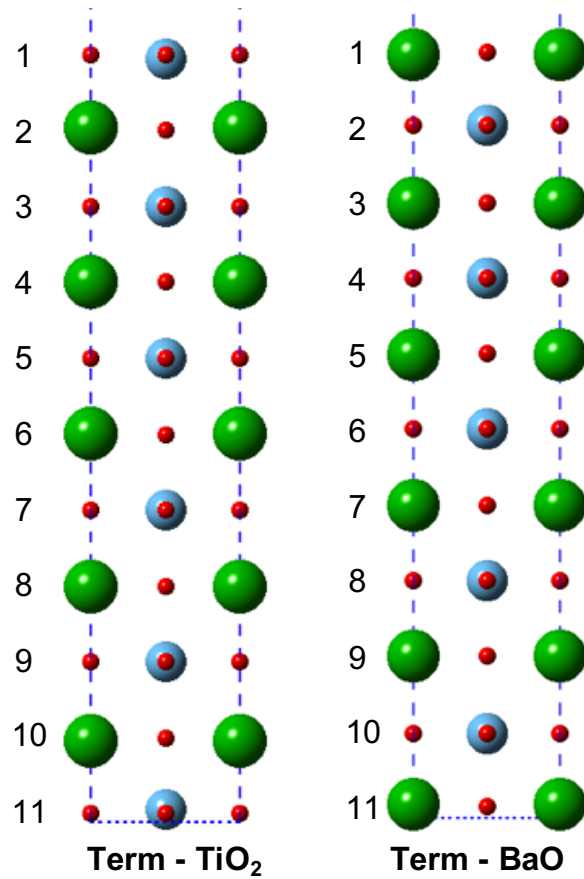


Figure 1: Side views of BaTiO₃ structures for (Left) the TiO₂ termination and (Right) the BaO termination. Ba atoms are reported in green, Ti in blue and oxygen in red. Layers are numbered according to numbers reported on the left.

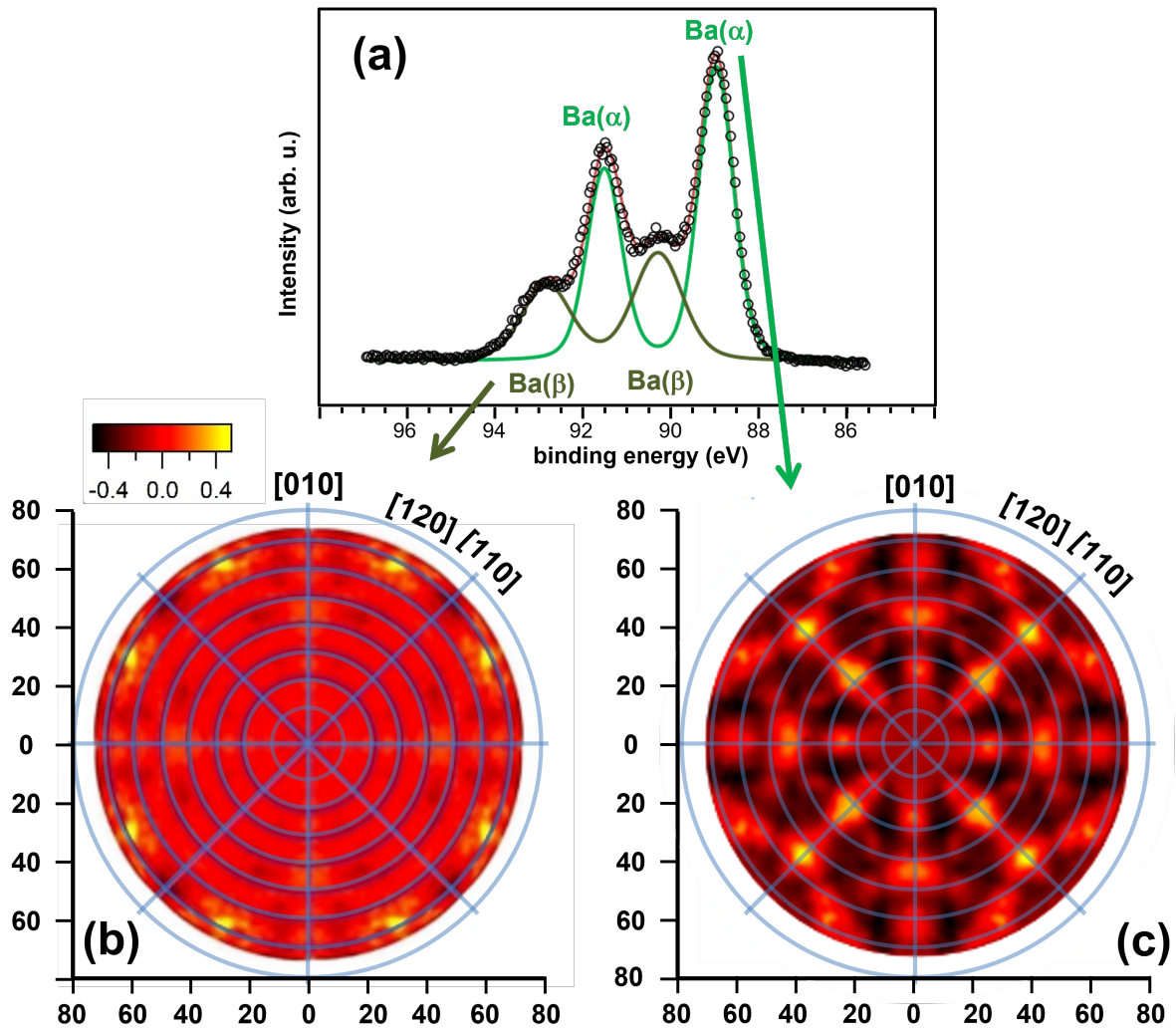


Figure 2: Ba 4d spectrum (a) obtained from sample S(0). Ba 4d lines are decomposed in two pairs of components: Ba(α) and Ba(β) Diffraction patterns recorded for components (b) Ba(β) and (c) Ba(α) are also presented. For these measurements, the photon energy is set at 547 eV

composed into two components named here Ba(α) and Ba(β) showing a BE shift of 1.25 eV. One should also underline that the FWHM of Ba(β) is significantly larger than the one of Ba(α). These two observations are in agreement with previous findings.¹² The shift between Ba(α) and Ba(β) is the issue of this paper and will be discussed in the following. Concerning the FWHM difference, one should keep in mind that the FWHM value is function of several parameters such as the used instrument (X-ray source, analyzer, ...), the average lifetime of the electron hole related to the photoemission process and the distribution of chemical states of the considered element. In our study, the first two parameters are identical for Ba(α) and Ba(β) components. The FWHM difference should thus be due to a noticeable change in the distribution of chemical states between Ba(α) and Ba(β). This point will be addressed at the end of the discussion. Concerning the coexistence of two Ba components, in the literature, basically two points of view arise about the interpretation of the corresponding barium chemical state. On one hand,^{10,12} the high energy component is attributed to surface states, while the low energy one is attributed to bulk atoms, but with no clear limit for bulk *vs.* surface atoms. On the other hand, the peak of higher energy is attributed to BaCO₃ species associated with a certain degree of surface contamination.^{13,14} Finally, a few alternative studies attributed the splitting to the formation of BaO₂¹⁷ species or to the existence of domains with different polarizations.³⁴

The presence of barium carbonate is an hypothesis that can be easily discarded in an UHV environment, since the preparation procedure yields a clean surface. Eventually, after prolonged sets of measurements (e.g. overnight PED scans) one may find the appearance of a faint C 1s component which is however located at a BE of 284.5 eV, corresponding to a standard adventitious peak (carbon species from the residual gas pressure) and not to the formation of a carbonate compound.

To disentangle the different structural environments associated with the two spectroscopic components (Ba(α) and Ba(β)) within the BaTiO₃ crystalline film, we measured the Ba 4d photoemission intensity with high angular resolution (acceptance angle of 1.5°, FWHM)

at different azimuthal orientations of the sample ϕ and emission (polar) angles θ of the spectrometer. To do this, the complete Ba $4d$ spectrum is recorded for each pair of angular positions (θ, ϕ) , then each peak is decomposed into two components Ba(α) and Ba(β) (Figure 2(a)) and the patterns are separately constructed for each of these components by plotting the corresponding χ function. The two PED patterns are plotted on Figures 2(b) and (c). Figure 2(c) is related to the Ba(α) component and reveals intense modulations of the signal corresponding to the main bulk symmetry directions of the single crystal and are indicative of the very well crystallized structure of the BaTiO₃ film. Five intense features can be easily distinguished: three along the [100] (or [010]) direction corresponding to polar angles equal to *ca.* 26°, 45° and 63° and two along the [110] direction for polar angles equal to *ca.* 35° and 55°.

In a simple but meaningful approach, we attribute these five features to directions joining an emitting barium atom to close neighbors with strong scattering power. Within BaTiO₃, the atoms with the highest scattering power are the barium atoms ($Z=56$, vs $Z=22$ for Ti and $Z=8$ for O). Figure 3 shows schematic representations of the (010), (1-10) and (2-10) planes containing barium atoms. The directions joining several barium atoms are indicated with the angles they form with the normal to the surface. The five selected directions are fully compatible with the peaks observed in Figure 2(c). A sixth intense feature can be seen in Figure 2(c). It is located between the [100] and [110] directions, at *ca.* 27° from the [100] direction and for a polar angle close to 66°. This peak corresponds to a direction joining two barium atoms through an oxygen atom, located along the [120] direction and for a polar angle of 65.9° (Figure 3 - right). Hence, according to Figure 3, diffraction processes behind peaks observed on the Ba(α) diffraction pattern are related to barium atoms under at least two crystal planes: a TiO₂ plane but also a BaO plane. Thus, it appears that the Ba(α) component corresponds to barium atoms buried under the surface of the material. It should also be noted that the direction normal to the surface is partly made up of "columns" of barium atoms. In this direction an important diffraction process must also take place but is

not revealed by the diffraction pattern because of the method of normalization of the signals used (see experimental section).

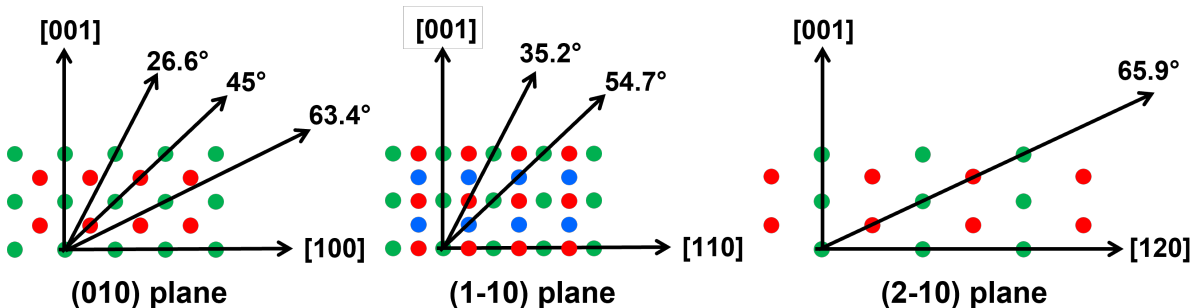


Figure 3: Schematic representation of the (010), (1-10) and (2-10) planes containing barium atoms. Ba atoms are in green, oxygen in red and titanium in blue. Main directions joining Ba atoms are indicated with the related polar angle

The diffraction pattern recorded from the Ba(β) component (Figure 2(b)) is radically different. According to the directions [100] and [110], no feature really appears in the diffraction pattern. This may be due to a large crystallographic disorder around the emitting atoms or, more likely, to the absence of a scattering atom above the emitting atoms. In the latter case, any angular modulation of the pattern could only be originated by photoelectrons backward scattered by the atoms beneath the emitter, a process almost negligible at such an electron kinetic energy (455 eV). In fact, only a few faint features are observed close to the surface horizon (grazing emission), which can be associated with intra-layer (forward) scattering of the surface atoms (e.g. due to a small rippling). Thus, it appears that the Ba(β) component cannot emanate from any other atom than those present in the top surface BaO plane. Despite it is beyond the scope of this study and an accurate refinement would be a complete study by itself,^{35,36} multiple scattering calculations have been performed through the EDAC code³⁷ for the bulk and the surface of a BaO terminated sample. Obtained diffraction patterns of the Ba 4*d* emitter are reported in SI and confirm the qualitative attribution discussed above.

Calculations results

To go further in this attribution, DFT calculations of Core Level Binding Energy (CLBE) shifts were performed on two different systems, namely BaTiO_3 with either a TiO_2 or a BaO termination (see Figure 1). As mentioned in computational details, the used method does not allow to calculate absolute CLBE, but only CLBE differences. Hence, for both terminations, we report on Figure 4, the evolution of δ_{CLBE} , with δ_{CLBE} calculated as follows: for a given layer n , $\delta_{CLBE}(n) = \text{CLBE}(n) - \text{CLBE}_{ref}$, with CLBE_{ref} corresponding to the CLBE of the central layer, namely layer 6 for the TiO_2 termination and average value of layers 5 and 7 for BaO termination. Only BaO layers are reported, where the even numbers correspond to the BaO layers in the slab terminated by TiO_2 termination (both sides) and odd numbers are the BaO layers in the slab terminated by BaO (both sides), according to numbering of Figure 1. From results reported on Figure 4, two distinct behaviors occur

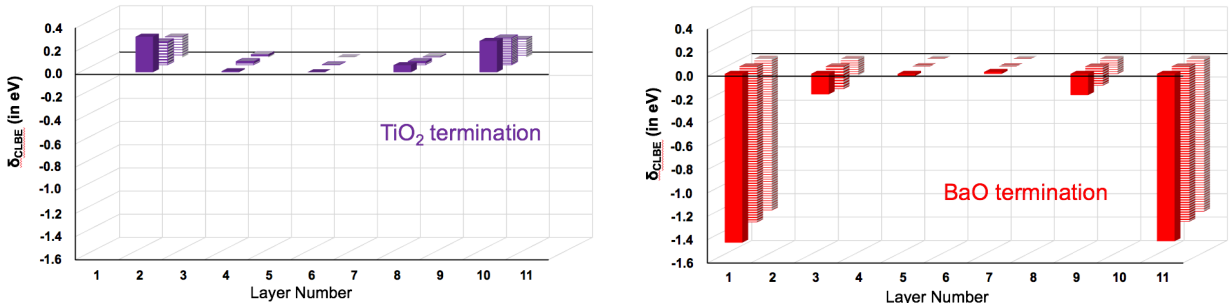


Figure 4: Evolution of δ_{CLBE} (in eV) of the Ba $4d$ level as a function of the layer number (see Figure 1 for numbering). Values for the TiO_2 termination are reported in purple on left panel, while ones for BaO are in red on the right panel. Plain bars stand for the native (1×1) cell, while bold lined and light lined bars stand for (2×1) and (2×2) cells, respectively.

for the two terminations. While values below 0.3 eV are calculated for all Ba atoms of the slab with TiO_2 terminations (see Figure 4 – Left), two sets of values are predicted for the slab with BaO terminations (see Figure 4 – Right). A δ_{CLBE} of -1.4 eV is calculated for the Ba atoms in the two terminal layers (1 and 11), while a δ_{CLBE} below -0.2 eV is found for all the inner layers (3,5,7,9). Even though only initial state effects are considered in this theoretical approach, the calculated core level shift of ~ 1.4 eV between the surface

layer and the buried ones in the BaO terminated slab is in very good agreement with the experimental shift of 1.25 eV between the Ba(α) and Ba(β) components, as well as with previous results.^{10,12} Conversely, only one component is predicted for a TiO₂ terminated slab, while experimentally the two components with the same shift are observed, independently of the sample preparation procedure.

In order to exclude possible artifacts in the calculations outcome, like boundaries effects related to the small cell size, the same calculations have been performed for a (2×1) and a (2×2) cell, with results also reported on Figure 4, with lined bars. According to these calculations, whatever the size of the calculation cell, two sets of values are obtained for the BaO terminated cells and only one for the TiO₂ ones.

To conclude on our theoretical results, the experimentally observed Ba(β) peak can only be assigned to the topmost BaO layer. As an interesting but surprising consequence, no Ba(β) signal should be observed for an experimental sample terminated by a complete layer of TiO₂.

SR-PES results

Association of photoelectron diffraction and DFT calculations suggests that for the (001) surface of BaTiO₃, the Ba(β) component of the Ba 4*d* spectrum is only related to the presence of a surface BaO atomic plane. The fact that experimentally all samples present both Ba(α) and Ba(β) signals, indicates that the surface of all samples is covered (at least partially) by a BaO layer. Consequently, we propose to interpret the ratios of Ba(α) and Ba(β) signals of various samples in terms of the fraction γ (from 0 to 1) of the surface covered by a BaO termination. It will be the purpose of the following part.

As the highlighted effect is located within the last atomic layer, experimental conditions as sensitive as possible to the surface have been used. In particular, analysis performed with a photon excitation energy of 160 eV and a low collection angle (15°) greatly limit the energy of the emitted electrons and thus their IMFP. Thanks to these experimental conditions, the

analysis is localized to the very first atomic layers. In this framework, Figure 5 reports the Ba 4*d* spectra of samples S(Ba_1) and S(Ti_1). In each case, Ba 4*d* lines can be still decomposed into two pairs of components showing a shift of *ca.* 1.25 eV. The decomposition of the spectra is performed by means of casaXPS software. A Gaussian–Lorentzian line shape GL(30) was employed to fit the XPS peaks after background subtraction based on the Shirley algorithm. The fit constraints are (0.9 ± 0.05) eV for FWHM of α components, (1.35 ± 0.05) eV for FWHM of β components as well as a spin-orbit splitting of 2.6 eV. In these experimental conditions, the Ba(β) contribution is largely dominant. It is worth noting that at grazing emission the electronic signal is less disturbed by forward scattering diffraction processes. Especially, if one was to consider a normal emission at the surface, an important diffraction process could modify the intensity of the signal emitted by the subsurface BaO planes. Besides, one has to specify that the determination of the BaO overlayer thickness is carried out by considering the Ba(α) and Ba(β) contributions which correspond to electrons of (very) similar kinetic energy, constituting the same line (Ba4*d*). Detector non-linearity can thus be safely neglected.

Following our hypothesis of a Ba(β) contribution only due to surface BaO, we simulate the ratio of Ba(β) and Ba(α) intensities measured for the 4 samples (Table 1). We use the classical method proposed by Fadley,³⁸ adapted to the BaTiO₃(001) surface. For this purpose, the material is decomposed into a sequence of alternating BaO and TiO₂ planes, for a total of 9 planes (Figure 6). The BaO surface plane, covers the underlying TiO₂ plane with a tunable coverage rate (γ) which will be the only fitting parameter of the model. The proposed model can simply be interpreted as a solid with two domains: one with a BaO termination occupying a proportion γ of the material surface and the other one with a TiO₂ termination occupying a proportion $1 - \gamma$. The respective thicknesses of the BaO and TiO₂ planes are arbitrarily set at half of the lattice parameter ($a/2 = 0.205$ nm), while the IMFP of the electrons crossing the different layers are determined from the TPP formula. For

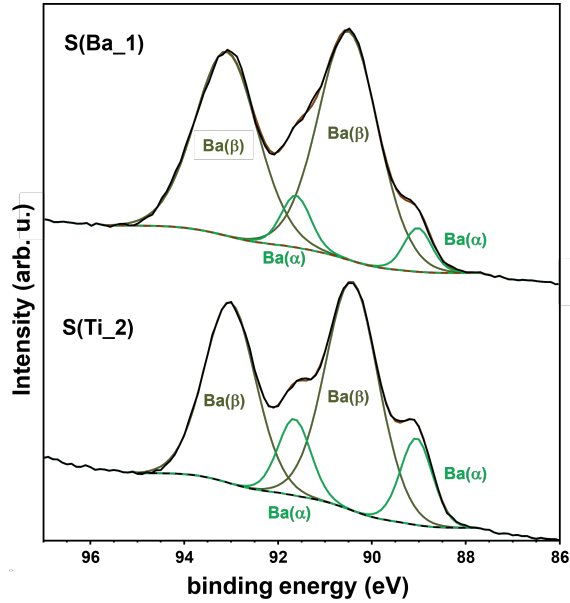


Figure 5: Ba 4d spectra obtained from two samples (Ba rich termination for S(Ba_1); Ti rich termination for S(Ti_2)). Ba 4d lines are decomposed in two pairs of components: α (light green) and β (dark green). Photon energy is 160 eV and the emission angle is 15° from the surface

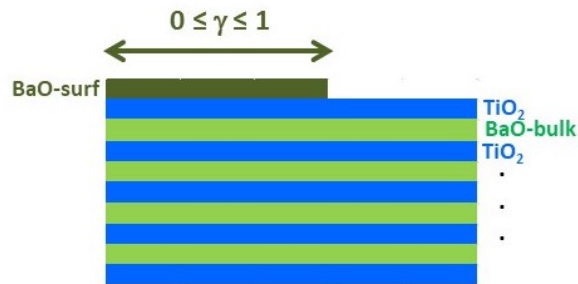


Figure 6: Decomposition of the material into a sequence of BaO and TiO₂ planes used for the refinement of photoemission data through a model material. The tunable cover rate (γ) is the only fitting parameter

electrons having a kinetic energy of *ca.* 75 eV, the IMFP is $\lambda_{BaO} = 0.49$ nm in BaO and is $\lambda_{TiO_2} = 0.54$ nm in TiO₂. Finally, since each BaO or TiO₂ plane is of monoatomic thickness, we consider that the electrons are not absorbed by the planes from which they are emitted. Calculations considering only the intensity of the barium peaks makes it possible to get rid of the ionization cross sections which are always tricky to determine, especially close to the ionization threshold. We apply the same IMFP for Ba(α) and Ba(β) electrons and we ensure that this description of the sample is thick enough by comparison of the detected intensity from the first BaO plane with that from the fifth BaO plane: in the least favorable case (low BaO coverage), this ratio is over 10,000 demonstrating that it is not useful to consider a thicker material. These assumptions greatly simplify the model. The results of the refinements through BaO coverage parameter are reported in Table 2. They demonstrate that

Table 2: Values of the experimental Ba(β)/Ba(α) ratio and coverage rate obtained by refinement from the model shown on Figure 6.

Sample	Experimental Ba(β)/Ba(α) ratio	BaO coverage (γ)
S(Ti_1)	3.12	0.47
S(Ti_2)	3.95	0.54
S(Ba_1)	14.25	0.92
S(Ba_2)	15.50	0.94

the proposed model allows to determine a BaO coverage in agreement with the experimental Ba(β)/Ba(α) ratio. This validates our hypothesis that the Ba(β) contribution is only related to the surface molecular layer of BaO. In particular, no other model allows to fit the experimental results. Other models were tested to reproduce the ratios, including placing a part of the emitter layer of the Ba(β) signal under a TiO₂ plane. Especially, for one of the tested models, to simulate the intensity of Ba(β) we added the signal emitted by the surface BaO to the one coming from the part of the first atomic plane of bulk BaO covered only by a plane of TiO₂. None of these tests were self consistent and did not even come close to the measured ratio values.

Our crossed experimental and theoretical investigation assigns the Ba(β) component only

to a surface BaO plane. The Ba(α) component thus corresponds to barium atoms present in well determined crystallographic sites of BaTiO₃ bulk. The chemical bonds that these atoms make with their environment are strictly the same for each atom and this does not lead to any kind of chemical state distribution. On the other hand, Ba(β) component is related to atoms forming a surface plane of BaO where the bonds are less unique in the sense that there is a form of pending bonds that must be compensated in several ways. It is, probably, this effect that induces a broadening of the Ba(β) component compared to Ba(α) component. It should also be noted that, like the Ba(α) component, the Ba(β) component is strictly symmetrical, which indicates a continuity of chemical states around an average chemistry and not several distinct chemical states.

Our conclusion, that Ba(β) comes only from a topmost layer of BaO, raises the debate of the systematic presence of the Ba(β) component, even for Ti-rich sample. This is explain by our fine spectroscopical analysis that indicates that titanium rich terminations are never pure and always contain a large fraction (the minimum value obtained here is 47%) of superficial BaO.

Conclusion

To investigate the nature of the BaTiO₃ Ba 4*d* splitting, we performed two sets of experiments on (001) epitaxial and therefore monocrystalline thin films using synchrotron radiation photoemission techniques (PED and SR-PES) supported by DFT calculations.

The photoelectron diffraction and low energy photoemission measurements in conditions of maximum surface sensitivity (in terms of photoelecron escape depth), demonstrate that the Ba 4*d* photoemission peak from the BaO surface layer presents a marked shift (*ca.* 1.25 eV towards higher binding energies) with respect to the signals coming from subsurface layers. This is quantitatively supported by DFT calculations, which confirm that i) the BE value of

Ba 4*d* is practically the same (within ± 0.10 eV) for all buried layers, and ii) only the Ba 4*d* peak of an uncovered surface layer is shifted to a much larger BE value, in full agreement with XPS evidences.

The extrapolation of these results offers a solid basis to study the behavior of BaTiO₃ surfaces in more realistic situations. Importantly, our approach and model demonstrate that the compositional state of a BaTiO₃ surface can be retrieved simply from the Ba(β) / Ba(α) photoemission intensities ratios.

Controlling and checking the surface plane of the ferroelectric compound BaTiO₃ is very important to understand its catalytic activity, its screening efficiency of ferroelectric polarisation and more generally its physical properties.

Supporting Information Available

Experimental and theoretical Ba 4*d* diffraction patterns for Ba(β) and Ba(α) components.

Acknowledgement

Calculations were performed using HPC resources from DNUM CCUB (Centre de Calcul de l'Université de Bourgogne). This work was also granted access to the HPC resources of IDRIS under the allocation 2021-A0110811108 made by GENCI. The authors also thank the ANR for financial support through project ANR-17-EURE-0002 (EIPHI Graduate School) and PHOTOPOT grant ANR-15-CE05-0014. The research leading to this result has been supported by the project CALIPSOplus under the Grant Agreement 730872 from the EU Framework Program for Research and Innovation HORIZON 2020.

References

- (1) Yamamoto, S.; Andersson, K.; Bluhm, H.; Ketteler, G.; Starr, D.; Schiros, T.; Ogasawara, H.; Pettersson, L.; Salmeron, M.; Nilsson, A. Hydroxyl-Induced Wetting of Metals by Water at Near-Ambient Conditions. *J. Phys. Chem. C* **2007**, *111*, 7848–7850.
- (2) Ackermann, M.; Pedersen, T.; Hendriksen, B.; Robach, O.; Bobaru, S.; Popa, I.; Quiros, C.; Kim, H.; Hammer, B.; Ferrer, S.; Frenken, J. Structure and Reactivity of Surface Oxides on Pt(110) during Catalytic CO Oxidation. *Phys. Rev. Lett.* **2005**, *95*, 255505/1–255505/4.
- (3) Song, K.; He, F.; Zhou, E.; Wang, L.; Hou, H.; Yang, W. Boosting solar water oxidation activity of BiVO₄ photoanode through an efficient in-situ selective surface cation exchange strategy. *J. Energy Chem.* **2022**, *68*, 49–59.
- (4) Finocchi, F.; Barbier, A.; Jupille, J.; Noguera, C. Stability of Rocksalt (111) Polar Surfaces: Beyond the Octopole. *Phys. Rev. Lett.* **2004**, *92*, 136101/1–136101/4.
- (5) Barbier, A.; Stierle, A.; Finocchi, F.; Jupille, J. Stability and stoichiometry of (polar) oxide surfaces for varying oxygen chemical potential. *J. Phys.: Condens. Matter* **2008**, *20*, 184014/1–184014/13.
- (6) Barbier, A.; Stierle, A.; Kasper, N.; Guittet, M.; Jupille, J. Surface termination of hematite at environmental oxygen pressures: Experimental surface phase diagram. *Phys. Rev. B* **2007**, *75*, 233406/1–233406/4.
- (7) Barbier, A.; Mocuta, C.; Neubeck, W.; Mulazzi, M.; Yakhou, F.; Chesnel, K.; Sollier, A.; Vettier, C.; de Bergevin, F. Surface and Bulk Spin Ordering of Antiferromagnetic Materials: NiO(111). *Phys. Rev. Lett.* **2004**, *93*, 257208/1–257208/4.

- (8) von Hippel, A.; Breckenridge, R.; Chesley, F.; Tisza, L. High dielectric constant ceramics. *Ind. Enf. Chem.* **1946**, *38*, 1097–1109.
- (9) Hudson, L.; Kurtz, L.; Robey, S.; Temple, D.; Stockbauer, R. Surface core-level shifts of barium observed in photoemission of vacuum-fractured BaTiO₃(100). *Phys. Rev. B* **1993**, *47*, 10832–10838.
- (10) Mukhopadhyay, S.; Chen, T. Surface chemical states of barium titanate: Influence of sample processing. *J. Mater. Res.* **1995**, *10*, 1502–1507.
- (11) Wang, J.; Gaillard, F.; Pancotti, A.; Gautier, B.; Niu, G.; Vilquin, B.; Pillard, V.; Rodrigues, G.; Barrett, N. Chemistry and Atomic Distortion at the Surface of an Epitaxial BaTiO₃ Thin Film after Dissociative Adsorption of Water. *J. Phys. Chem. C* **2012**, *116*, 21802–21809.
- (12) Pancotti, A.; Wang, J.; Chen, P.; Tortech, L.; Teodorescu, C.-M.; Frantzeskakis, E.; Barrett, N. X-ray photoelectron diffraction study of relaxation and rumpling of ferroelectric domains in BaTiO₃(001). *Phys. Rev. B* **2013**, *87*, 184116/1–184116/10.
- (13) Fujisaki, Y.; Shimamoto, Y.; Matsui, Y. Analysis of Decomposed Layer Appearing on the Surface of Barium Strontium Titanate. *Jpn. J. Appl. Phys.* **1999**, *38*, L52–L55.
- (14) Craciun, V.; Singh, R. Characteristics of the surface layer of barium strontium titanate thin films deposited by laser ablation. *App. Phys. Lett.* **2000**, *76*, 1932–1934.
- (15) Li, C.; Chang, S.; Lee, J.; Liao, W. Efficient hydroxylation of BaTiO₃ nanoparticles by using hydrogen peroxide. *Colloids Surf. A: Physicochem. Eng. Asp.* **2010**, *361*, 143–149.
- (16) Barbier, A.; Mocuta, C.; Stanescu, D.; Jegou, P.; Jedrecy, N.; Magnan, H. Surface composition of BaTiO₃/SrTiO₃(001) films grown by atomic oxygen plasma assisted molecular beam epitaxy. *J. Appl. Phys.* **2012**, *112*, 114116–114118.

- (17) Droubay, T.; Kong, L.; Chambers, S.; Hess, W. Work function reduction by BaO: Growth of crystalline barium oxide on Ag(001) and Ag(111) surfaces. *Surf. Sci.* **2015**, *632*, 201–206.
- (18) Chakrabarti, S.; Ginnaram, S.; Jana, S.; Wu, Z.; Singh, K.; Roy, A.; Kumar, P.; Maikap, S.; Qiu, J.; Cheng, H.; *et al.*, Negative voltage modulated multi-level resistive switching by using a Cr/BaTiO_x/TiN structure and quantum conductance through evidence of H₂O₂ sensing mechanism. *Sci. Rep.* **2017**, *7*, 4735/1–4735/13.
- (19) Spasojevic, I.; Sauthier, G.; Caicedo, J.; Verdaguer, A.; Domingo, N. Oxidation processes at the surface of BaTiO₃ thin films under environmental conditions. *App. Surf. Sci.* **2021**, *565*, 150288/1–150288/9.
- (20) Magnan, H.; Deleuze, P.; Brehin, J.; Plays, T.; Stanescu, D.; Flavell, W.; Silly, M.; Domenichini, B.; Barbier, A. Tuning the Charge Carriers Migration in Epitaxial BaTiO₃ Thin-Film Photoanodes. *J. Phys. Chem. C* **2020**, *124*, 10315–10323.
- (21) Floreano, L.; Naletto, G.; Cvetko, D.; Gotter, R.; Malvezzi, M.; Marassi, L.; Morgante, A.; Santaniello, A.; Verdini, A.; Tommasini, F.; *et al.*, Performance of the grating-crystal monochromator of the ALOISA beamline at the Elettra Synchrotron. *Rev. Sci. Instrum.* **1999**, *70*, 3855–3864.
- (22) Bruno, F.; Floreano, L.; Verdini, A.; Cvetko, D.; Gotter, R.; Morgante, A.; Canepa, M.; Terreni, S. Study of the isotropic contribution to the analysis of photoelectron diffraction experiments at the ALOISA beamline. *J. Electron Spectrosc. Relat. Phenom.* **2002**, *127*, 85–92.
- (23) Kresse, G.; Furthmüller, J. Efficiency of ab-initio Total Energy Calculations for Metals and Semiconductors using a Plane-Wave Basis Set. *Comput. Mater. Sci.* **1996**, *6*, 15–50.
- (24) Kresse, G.; Furthmüller, J. Efficient Iterative Schemes for ab initio Total-Energy Calculations using a Plane-Wave Basis Set. *Phys. Rev. B* **1996**, *54*, 11169–11186.

- (25) Blöchl, P. Projector augmented-wave method. *Phys. Rev. B* **1994**, *50*, 17953–17979.
- (26) Kresse, G.; Joubert, D. From Ultrasoft Pseudopotentials to the Projector Augmented-Wave Method. *Phys. Rev. B* **1999**, *59*, 1758–1775.
- (27) Perdew, J.; Burke, K.; Ernzerhof, M. Generalized Gradient Approximation Made Simple. *Phys. Rev. Lett.* **1996**, *77*, 3865–3868.
- (28) Dudarev, S. L.; Botton, G. A.; Savrasov, S. Y.; Humphreys, C. J.; Sutton, A. P. Electron-Energy-Loss Spectra and the Structural Stability of Nickel Oxide: An LSDA+U study. *Phys. Rev. B* **1998**, *57*, 1505–1509.
- (29) Suzuki, K.; Kijima, K. Optical Band Gap of Barium Titanate Nanoparticles Prepared by RF-plasma Chemical Vapor Deposition. *Jpn. J. Appl. Phys.* **2005**, *44*, 2081–2082.
- (30) Pack, J.; Monkhorst, H. "Special points for Brillouin-zone integrations"—a reply. *Phys. Rev. B* **1977**, *16*, 1748–1749.
- (31) Deleuze, P.; Mahmoud, A.; Domenichini, B.; Dupont, C. Theoretical investigation of the platinum substrate influence on BaTiO₃ thin film polarisation. *Phys. Chem. Chem. Phys.* **2019**, *21*, 4367–4374.
- (32) Köhler, L.; Kresse, G. Density functional study of CO on Rh(111). *Phys. Rev. B* **2004**, *70*, 165405/1–165405/9.
- (33) Tanuma, S.; Powell, C.; Penn, D. Calculations of electron inelastic mean free paths. V. Data for 14 organic-compounds over the 50-2000 eV range. *Surf. Interf. Anal.* **1994**, *21*, 165–176.
- (34) Kumar, S.; Raju, V.; Kutty, T. Investigations on the chemical states of sintered barium titanate by X-ray photoelectron spectroscopy. *App. Surf. Sci.* **2003**, *206*, 250–261.

- (35) Dupont, C.; Bourgeois, S.; Le Fèvre, P.; Verdini, A.; Floreano, L.; Domenichini, B. Structure of TiO₂ (011) Revealed by Photoelectron Diffraction. *Phys. Rev. B* **2016**, *94*, 241304(R)/1–241304(R)/6.
- (36) Dupont, C.; Jupille, J.; Bourgeois, S.; Le Fèvre, P.; Verdini, A.; Floreano, L.; Domenichini, B. Substitution of Titanium for Magnesium Ions at the Surface of Mg-Doped Rutile. *J. Phys. Chem. C* **2020**, *124*, 11490–11498.
- (37) Garcia de Abajo, F.; Van Hove, M.; Fadley, C. Multiple scattering of electrons in solids and molecules: A cluster-model approach. *Phys. Rev. B* **2001**, *63*, 075404/1–075404/16.
- (38) Fadley, C. Angle-resolved x-ray photoelectron spectroscopy. *Prog. Surf. Sci.* **1984**, *16*, 275–388.

TOC Graphic

